Mineralogy and Petrology (2019) 113:613–623
https://doi.org/10.1007/s00710-019-00672-0

ORIGINAL PAPER

Compressibility and structure behaviour of maruyamaite (K-tourmaline) from the Kokchetav massif at high pressure up to 20 GPa

Anna Yu. Likhacheva[1] · S. V. Rashchenko[1,2] · Kira A. Musiyachenko[1] · Andrey V. Korsakov[1] · Ines E. Collings[3] · Michael Hanfland[3]

Received: 21 January 2019 / Accepted: 7 June 2019 / Published online: 22 June 2019

Abstract

The structural behaviour of maruyamaite (K-dominant tourmaline) $^{X}(K_{0.54}Na_{0.28}Ca_{0.19})^{Y}(Mg_{1.3}Al_{1.17}Fe_{0.39}Ti_{0.14})^{Z}(Al_5Mg)[Si_{5.95}Al_{0.05}O_{18}](BO_3)_3{}^{V,W}[O_{1.69}(OH)_{2.31}]$ from the ultrahigh-pressure metamorphic rocks of Kokchetav massif was studied using synchrotron based single-crystal diffraction up to 20 GPa. Within the whole pressure range the compression is regular and anisotropic, with the c direction being more compressible than the a direction. Fitting the V/*P* data with the 2nd and 3rd order Birch-Murnaghan equations of state gives: $V_0 = 1587.2(7)$ Å^3, $K_0 = 115.6(9)$ GPa at fixed $K' = 4$, and $V_0 = 1588(1)$ Å^3, $K_0 = 112(3)$ GPa, $K' = 4.5(4)$. The bulk modulus values are slightly higher as compared to those found for dravite and cation-deficient synthetic K-dravite. The pressure evolution of the main structural parameters of K-tourmaline is similar to those of dravite. However, a minor change in the rigidity of local contacts of the *X* site with 6-membered ring, due to the presence of K, is apparently critical for stabilization of tourmaline structure within 15–20 GPa, which is evinced by the absence of the phase transition observed in dravite near 15.4 GPa. The stabilizing function of K becomes apparent at $P > 15$ GPa. The comparison of the H*P* structural behaviour of maruyamaite and dravite supports the recent suggestion that the large *X* site plays a secondary role in the elastic behaviour of tourmaline, compared to the octahedral framework. In addition, the present study reveals several new features of polyhedra distortions, which demonstrate their complex interaction on compression.

Keywords Maruyamaite · K-tourmaline · High pressure · single-crystal diffraction · crystal structure refinement · Kokchetav Massif · northern Kazakhstan · UHP metamorphism

Introduction

Tourmaline, the most abundant borosilicate mineral in the Earth's crust (Henry and Dutrow 1996), is prominent due to its chemical complexity and diversity of natural occurrences, including metamorphic rocks, pegmatites, ore deposits, etc. (Dutrow and Henry 2011; Martin 2011). Chemical variability and stability in a wide *P-T* range make tourmaline a powerful petrogenetic indicator of chemistry (e.g., Henry and Dutrow 1996; Lussier et al. 2008, 2011; Lussier and Hawthorne 2011; Dutrow and Henry 2011; Hawthorne and Dirlam 2011; van Hinsberg et al. 2011; Novák et al. 2011) and isotopic composition (e.g., Marschall et al. 2006; Marschall and Jiang 2011; Meyer et al. 2008; Ludwig et al. 2011; Hezel et al. 2011) of its host rocks.

The crystal structure of tourmaline supergroup minerals with general formula $^{[9]}X^{[6]}Y_3{}^{[6]}Z_6(T_6O_{18})(BO_3)_3V_3W$

Editorial handling: S. W. Faryad

Electronic supplementary material The online version of this article (https://doi.org/10.1007/s00710-019-00672-0) contains supplementary material, which is available to authorized users.

✉ Anna Yu. Likhacheva
alih@igm.nsc.ru

[1] V.S. Sobolev Institute of Geology and Mineralogy SibD RAS, pr. ak. Koptyuga 3, 630090 Novosibirsk, Russia

[2] Novosibirsk State University, Pirogova str. 1, 630090 Novosibirsk, Russia

[3] European Synchrotron Radiation Facility, 71 Avenue des Martyrs, 38000 Grenoble, France

accommodates a large variety of elements, the main constituents being distributed as follows: X = Na, Ca, □ (vacancy); Y = Mg, Fe, Mn, Al, Li, Ti; Z = Al, Fe, Mg, Cr; T = Si, Al; B = B; V = OH, O; W = OH, F, O (Hawthorne and Henry 1999; Henry et al. 2011). The dominant constituents at the largest (nine-fold) X site are Na and Ca. Concerning K, it is found only in minor amounts and is mainly considered as incompatible in tourmaline, likely due to its larger ionic radius (1.55 Å in ninefold coordination) as compared to 1.24 Å for Na^+ (Shannon 1976). However, the incorporation of appreciable amounts of K in tourmaline at high pressure was predicted by thermodynamic modeling (van Hinsberg and Schumacher 2007). Indeed, K-dominant tourmaline (maruyamaite, the K-analogue of oxydravite containing K > Na + Ca) has been recently found in ultrahigh-pressure (UHP) diamondiferous gneisses of the Kokchetav Massif (Kumdy-Kol area, northern Kazakhstan) (Shimizu and Ogasawara 2005, 2013; Ota et al. 2008a, 2008b). Its ideal formula is $K(MgAl_2)(Al_5Mg)Si_6O_{18}(BO_3)_3(OH)_3O$, though the maximal K content does not exceed 0.583 per formula unit (pfu) (Shimizu and Ogasawara 2013). The experimental studies (Berryman et al. 2014, 2015) and the analysis of the Kokchetav rocks (Schertl and Sobolev 2013; Hwang et al. 2005) agree that maruyamaite was likely to form at UHP conditions, in the stability field of diamond (Ota et al. 2008a, 2008b) in the presence of K-rich fluid. Moreover, the K (and Na) contents of the Kokchetav tourmaline are shown to qualitatively constrain the metamorphic grade and composition of their formation environment (Berryman et al. 2015). This makes K-rich tourmaline a potentially important geobarometer and stimulates further studies of its structure properties and stability.

Tourmaline, a ring silicate, crystallizes in the trigonal space group $R3m$ (Foit 1989; Hawthorne and Henry 1999; Henry et al. 2011). The crystal structure (Fig. 1) is composed of 6-membered rings of corner-linked TO_4 tetrahedra (T site), each of them sharing an apex corner with one Y-site and one Z-site octahedron. The three edge-sharing Y octahedra lie below the ring and are surrounded by six Z octahedra. The ninefold X site, lying directly above the T_6O_{18} ring, is coordinated by the six inner corners of the T_6O_{18} ring and three inner corners of the upper trimer of Y octahedra. The single W (O1) site is found below the center of the T_6O_{18} ring, at the triple joint of the Y octahedra. The O1–H1 bond is oriented toward the X site.

The elastic behaviour of tourmaline as a function of the X-site composition is characterized by a pronounced anisotropy along the c-direction: a gradual volume increase due to the incorporation of a larger cation into the X site proceeds mainly through the lengthening of the crystallographic c-axis (Dietrich 1985; Berryman et al. 2016). Under high pressure the c direction also provides a pronounced anisotropy to the elastic behaviour of tourmaline: the compressibility along the

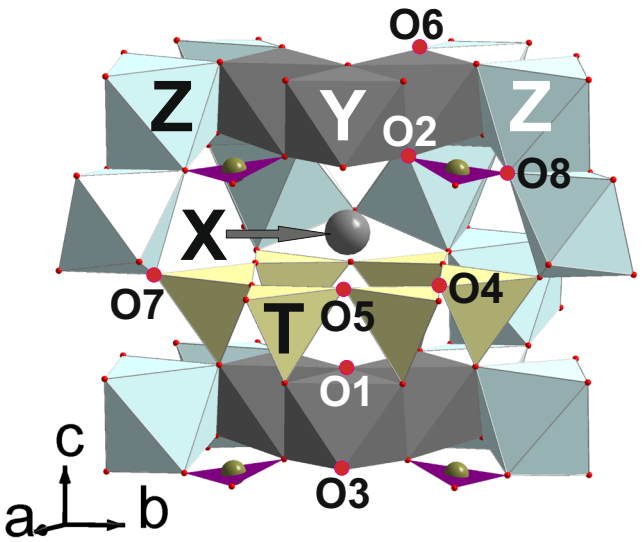

Fig. 1 Crystal structure of tourmaline, refined using the single-crystal data on maruyamaite collected at ambient pressure. The structural polyhedra and specific oxygen sites are labeled by larger and smaller letters, respectively. The BO_3 groups are shown as triangles

c axis is about 3 times larger as compared to the a axis (Li et al. 2004; Xu et al. 2016) and, for alkali tourmalines, tends to increase with the initial c dimension (Berryman et al. 2018). The recent comparative study of near end-member tourmalines reveals a critical role of the octahedral site composition for determining the resulting elastic properties, the highest bulk modulus of 124(7) GPa pertaining to olenite (Na-Al tourmaline) with the Y and Z sites fully occupied by Al (Berryman et al. 2018). The large X-site is found to have a secondary influence on tourmaline elasticity; however, the role of vacancies and different cations remains not well understood. Since the X polyhedron is shown to be the most compressible unit in tourmaline structure (O'Bannon et al. 2018), it seems important to elucidate the role of different cations in structural behaviour of tourmaline under pressure.

So far, only structure of dravite, ideally $(NaMg_3Al_6[Si_6O_{18}](BO_3)_3(OH)_3OH)$, was studied at high pressure using single crystal technique (O'Bannon et al. 2018). The Na-O1 distance (corresponding to the c-direction) is found to be almost twice as compressible compared to the other Na-O distances, which apparently contributes to a larger compressibility along the c axis. The compression mechanism involves a complex interplay of polyhedra deformation; for example, the contraction of the Y octahedra produces the puckering of the T_6O_{18} ring through the displacement of the O6 atom towards the threefold axis. Among the major pressure-induced effects is the increase of ditrigonality of the 6-membered rings, mainly under the influence of the X cation moving towards the ring. A minor transition accompanied by the symmetry reduction from $R3m$ to $R3$ is observed in dravite near 15.4 GPa. The HP phase is characterized by a distorted T_6O_{18} ring and by slight

change in the pressure dependence of several structural parameters.

The bulk modulus of synthetic K-dravite (112.0 GPa) is found to be slightly higher as compared to dravite (107 GPa) (Berryman et al. 2018). The aim of the present study is to examine how the replacement Na → K in dravitic tourmaline influences its structural behaviour at high pressure, with a particular attention to stabilizing function of a large K^+ cation. We report the results of single-crystal diffraction study of maruyamaite from the UHP rocks of Kokchetav massif at high pressure up to 20 GPa.

Experimental

The chemical composition of selected tourmaline grains from the UHP quartzofeldspathic rocks, collected by the authors in the Kumdy-Kol area of the Kokchetav Massif (the sample G270, Fig. 2), was analyzed by MIRA 3 LMU scanning electron microscope equipped with INCA Energy 450 XMax 80 microanalysis system. All the analyzed grains were chemically zoned, with the core domains enriched in K, in agreement with the data of Ota et al. (2008a, 2008b), Shimizu and Ogasawara (2013) and Lussier et al. (2016). In one of these grains the inner homogeneous zone, rich in K, was bounded by the cracks, which allowed us to detach it from the whole grain. Within the inner homogeneous zone the mean K content is 2.56 wt.% (≈ 0.55 per formula unit (pfu)), which allows us to classify it as maruyamaite (Ota et al. 2008a, 2008b; Shimizu and Ogasawara 2013; Lussier et al. 2016). A ~250 μm single-crystal fragment was extracted from the K-rich zone for high-pressure synchrotron X-ray diffraction experiments; its quality was checked using laboratory X-ray diffractometer STOE IPDS-2T.

The in situ H*P* single-crystal diffraction experiments were performed at the station ID015B at the European Synchrotron Radiation Facility. Membrane driven LeToullec type diamond anvil cell was used, equipped with Boehler-Almax anvils with an opening half-angle of 32°. The culet diameter was 600 μm. Stainless steel was used as the gasket material, indented to about 80 μm and drilled to obtain a sample chamber with diameter of 350 μm. A small chip of the above mentioned single-crystal fragment was placed inside the sample chamber along with ruby sphere. Hydrostatic conditions were provided

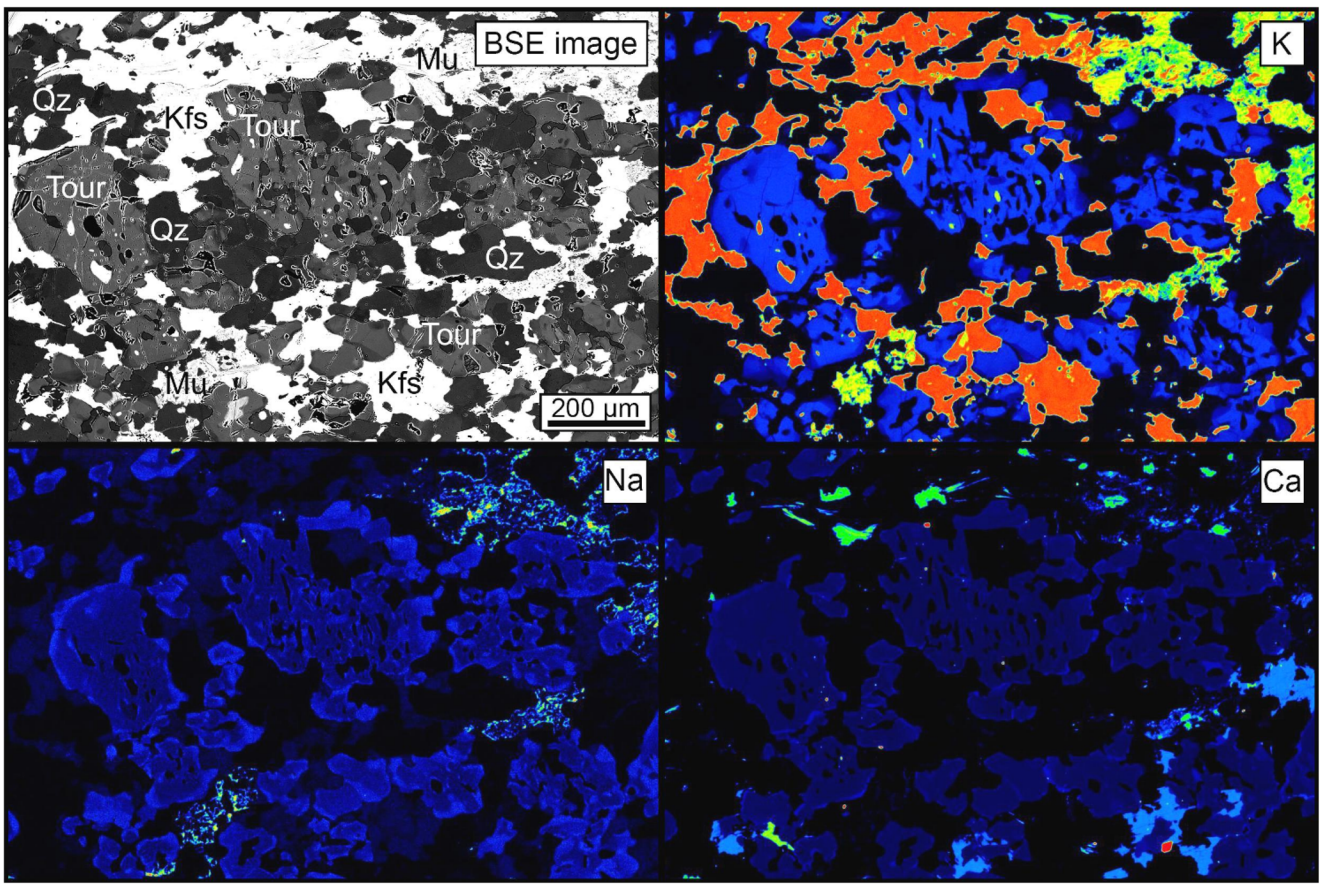

Fig. 2 BSE image and X-ray maps of element distribution in the group of tourmaline grains in the sample G270. Tourmalines display presence of the homogeneous high-K maruyamaite core with multiple quartz inclusions and thin Ca,Na-rich dravite rim. Mineral abbreviations: Kfs - K-feldspar, Mu- muscovite, Qz – quartz, Tour - tourmaline

by the DAC loading with a helium pressure-transmitting medium. Pressures were determined using ruby fluorescence scale (Mao et al. 1986). The zero-point measurement at ambient pressure was made first, and then the DAC was loaded with He and sequentially pressurized from 0.21 to 19.9 GPa.

Monochromatic X-ray diffraction measurements were performed at a wavelength of 0.41505 Å with a beam size of 10 × 10 μm (Merlini and Hafland 2013). Diffraction patterns were collected using a MAR555 flat panel detector during ±32 ° rotation of the DAC in 0.5 ° steps. The patterns were then transferred into CrysAlisPro software using ESPERANTO protocol (Agilent 2012; Rothkirch et al. 2013) for indexing and integration. A crystallographic computing system JANA2006 (Petříček et al. 2014) was used for structure refinement. Electron density of each mixed site was modelled by refinement of occupancy of its major constituent (K for X, Si for T, Al for Z, Mg for Y) using data measured at ambient conditions. The refined occupancies are 0.79, 0.95, 0.96, and 1.20, respectively, indicating the presence of Na in X site and Fe in Y site. The obtained values were then used in the structure refinement for all remaining pressure points.

The crystal structures were refined at 21 pressure points with anisotropic displacement parameters. The information on data collection and structure refinement (Table 1) and the CIF-files for all pressure points are attached to supplementary materials[1]. The selected structural parameters are given in Table 2. The unit-cell dimensions are given in Table 3.

Results

The chemical composition and crystal structure of maruyamaite

The average of 12 analyses on the K-rich inner homogeneous zone of tourmaline grain is: SiO_2 35.85 wt.%, Al_2O_3 31.80 wt.%, MgO 9.30 wt.%, FeO 2.81 wt.%, TiO_2 1.12 wt.%, K_2O 2.56 wt.%, Na_2O 0.87 wt.%, CaO 1.06 wt.%. The total sum is reduced to 85.37% due to the absence of determination of B and H_2O content. After the normalization to 15 cations at the *Y*, *Z*, and *T* sites (15*YZT*), and assuming B = 3 atoms per formula unit, we obtain the following preliminary formula: $^{X}(K_{0.54}Na_{0.28}Ca_{0.19})^{Y}(Mg_{2.3}Al_{0.17}Fe_{0.39}Ti_{0.14})^{Z}(Al_6)[Si_{5.95}Al_{0.05}O_{18}](BO_3)_3{}^{V,W}[O_{1.69}(OH)_{2.31}]$. We add the O^{2-} to meet the charge balance and merge it with OH^- into *V* and *W* site, since their real distribution is unknown.

In the structure solved at ambient pressure, the occupancies of cation polyhedra mentioned above fairly agree with the microprobe data (see CIFs). The mean *X*-O distance of 2.688 Å (Table 2) is close to that reported for maruyamaite (with *X* = 0.53 K + 0.26Ca + 0.19Na) from the same locality (Lussier et al. 2016). The mean *T*-O distance of 1.621 Å corresponds to the *T* site fully occupied by Si (MacDonald and Hawthorne 1995). The mean bond lengths in the YO_6 and ZO_6 octahedra (2.013 and 1.934 Å, Table 2) differ with those corresponding to the *Y* and *Z* sites fully occupied by Mg and Al (Hawthorne et al. 1993; Pertlik et al. 2003). Along with the measured Mg and Al contents, this indicates that there is Mg/Al disorder over the *Y* and *Z* sites. Such disorder, typical for Mg- and Al-bearing tourmalines, leads to the linear increase of the *Z*-O bond length from 1.904–1.910 Å for *Z* = Al6 to 1.932 Å for *Z* = Al5Mg (Hawthorne et al. 1993; Bloodaxe et al. 1999; Lussier et al. 2016). In the *Y* octahedron mainly occupied by Mg, the admixture of Al leads to the shortening of the average *Y*-O bond, compared to 2.045 Å typical for *Y* = Mg3 (Pertlik et al. 2003). Taking this into account, we finally obtain:

$^{X}(K_{0.54}Na_{0.28}Ca_{0.19})^{Y}(Mg_{1.3}Al_{1.17}Fe_{0.39}Ti_{0.14})^{Z}(Al_5Mg)[Si_{5.95}Al_{0.05}O_{18}](BO_3)_3{}^{V,W}[O_{1.69}(OH)_{2.31}]$.

The bond valence sums, derived from the presented formula following the approach of Hawthorne (2002), show a 12% over-bonding and 0.4% under-bonding at the *Y* and *Z* site, respectively. These values are in good agreement with the previous bond valence analyzes of dravite tourmalines (e.g. Hawthorne et al. 1993; O'Bannon et al. 2018).

Compressibility of maruyamaite up to 20 GPa

The unit cell parameters of maruyamaite at ambient pressure (Table 3) compare well with those of maruyamaite from the same locality (Lussier et al. 2016) and synthetic K-dravite (Berryman et al. 2016). The diffraction data collected up to 20 GPa show no deviation from the initial symmetry (space group *R*3*m*). To check this, we performed a trial refinement of dataset measured at 19.9 GPa, in the *R*3 space group, and found that shifts of atomic sites from special positions at mirror planes, characteristic for *R*3*m* space group, do not exceed 0.004 Å (estimated using PSEUDO routine – see Capillas et al. 2011; Sheldrick 2008).

The pressure dependences of the lattice parameters and volume are presented in Fig. 3 in comparison with the data on dravite (O'Bannon et al. 2018) and synthetic K-dravite (Berryman et al. 2018). Within the whole pressure range the compressibility is regular and anisotropic, the c direction being more compressible as compared to the ab plane. Fitting V/*P* data with the 2nd and 3rd order Birch-Murnaghan equations of state (Angel et al. 2014) gives: V_0 = 1587.2(7) Å^3, K_0 = 115.6(9) GPa at fixed K′ = 4, and V_0 = 1588(1) Å^3, K_0 = 112(3) GPa, K′ = 4.5(4). The comparison of the F-f plots (suppl. Fig. S1) shows that the 2nd order EoS provides a better fit of the experimental dataset. The obtained K_0 values are slightly higher as compared to those for dravite (K_0 = 112.0(1.0) GPa at fixed K′ = 4, and K_0 = 109.6(3.2) GPa at K′ = 4.4, after O'Bannon et al. (2018)) and synthetic K-

Table 1 Selected experimental data for maruyamaite (space group *R*3*m*) at high pressure

P, GPa	Crystal structure refinement					No. reflections for cell measurement
	No. unique reflections	No. variables	GOF	wR_{all} %	$R1_{all}$ %	
0.0001	563	91	1.42	4.71	4.58	324
0.21(1)	613	87	1.32	2.98	2.34	512
0.99(1)	642	87	1.31	2.73	2.15	523
2.04(1)	619	87	1.31	2.81	2.26	498
3.05(2)	636	87	1.38	2.74	2.18	530
4.06(1)	623	87	1.34	2.54	2.02	555
5.06(1)	651	87	1.37	2.57	2.02	552
6.10(2)	690	87	1.44	2.94	2.27	492
7.12(1)	682	87	1.40	2.91	2.28	467
8.13(1)	684	87	1.45	3.02	2.35	488
9.09(2)	682	87	1.61	3.09	2.33	555
10.06(2)	683	87	1.75	3.54	2.58	548
11.13(4)	603	87	1.41	3.00	2.27	427
12.20(5)	604	87	1.38	2.78	2.30	433
13.12(6)	599	87	1.40	2.73	2.37	448
14.06(5)	590	87	1.60	2.98	2.40	445
15.17(8)	579	87	1.43	2.79	2.35	436
16.07(9)	595	87	1.38	3.08	2.43	428
17.19(5)	609	87	1.76	3.17	2.43	459
17.94(3)	613	87	1.36	2.81	2.11	441
19.05(5)	619	87	1.44	2.84	2.34	442
19.9(1)	622	87	1.60	3.08	2.38	433
0.0001*	623	87	1.20	3.56	3.57	353

* after pressure release

dravite (K_0 = 112.0(0.5) GPa at fixed K′ = 4, and K_0 = 106(1.7) GPa at K′ = 4.5(2), after Berryman et al. (2018)). For the three presented tourmalines the c/c_0 dependences differ most distinctly, the axial compressibility slightly increasing in both K-varieties compared to dravite. To compare the compressibility of *a* and *c* parameters in maruyamaite, their cubed values were fitted to the 2nd order Birch-Murnaghan EoS to give: $K_{a(0)}$ = 181(2) GPa, $K_{c(0)}$ = 60.9(4) GPa (at fixed K′ = 4).

Structure evolution of maruyamaite at high pressure

The relative compressibilities of the main polyhedra in maruyamaite structure (Fig. 4, Table 2) are very similar to those found in dravite: *T* site is the most rigid, *X* polyhedron is the most compressible, and the *Y* and *Z* octahedra have intermediate compressibility. The V/*P* dependencies in Fig. 4 are rather smooth, in accordance with the regular H*P* behaviour of the lattice parameters. However, a minor but distinct anomaly of the V/*P* curves for SiO_4 (*T*) tetrahedron and *Y* octahedron is observed at about 10 GPa. A similar bend can be seen in the analogous dependences for dravite (O'Bannon et al. 2018) plotted in Fig. 4, despite a lower density of datapoints. The bulk compression of *T* polyhedron is almost identical for maruyamaite and dravite, neglecting the *T* site splitting described in dravite at *P* > 19 GPa (O'Bannon et al. 2018). The *Y* octahedron in maruyamaite contracts appreciably less than that in dravite; a small but distinct difference is also seen between the V/*P* trends for *Z* octahedron, which is more rigid in dravite.

Among the bonds entering the 9-fold coordination of the *X* site (K,Na) in maruyamaite, the *X*-O4 and *X*-O5 bonds with bridging O atoms of the T_6O_{18} ring behave differently under pressure (Fig. 5). Up to 20 GPa the *X*-O4 and *X*-O5 distances shorten by 1.2% and 11%, respectively; as a result, the ring ditrigonality increases (suppl. Fig. S2). From the nine bonds of the *X* site, only six bonds effectively participate in its compaction: three *X*-O5 bonds and three *X*-O2 bonds with the upper *Y* octahedra (Fig. 1), similarly to that observed in dravite (O'Bannon et al. 2018). Also, just as in dravite, the *X*-O1 distance is almost twice as compressible compared to the *X*-O bonds.

Despite the overall similarity in the H*P* evolution of *X* site in maruyamaite and dravite (Fig. 5), there are some

Table 2 Selected structural parameters of maruyamaite as a function of pressure

P, GPa	Puckering O6-L_3, Å	*X*-O2, Å	*X*-O1, Å	*X*-O4, Å	*X*-O5, Å	Crimping, Å	Ditrigonality	Polyhedron volume, Å^3			
								X-O_9	*Y*-O_6	*Z*-O_6	*T*-O_4
0.0001	3.030	2.558(5)	3.241(8)	2.782(5)	2.724(5)	0.12503	0.00078	32.3062	10.5421	9.4470	2.1747
0.21(1)	3.022	2.547(3)	3.224(6)	2.782(3)	2.704(3)	0.12608	0.00945	31.8499	10.5121	9.4134	2.1641
0.99(1)	3.018	2.541(3)	3.190(6)	2.778(3)	2.687(3)	0.13288	0.01461	31.4694	10.5061	9.3806	2.1647
2.04(1)	3.013	2.537(3)	3.167(6)	2.771(3)	2.674(3)	0.13195	0.01861	31.0526	10.4260	9.3085	2.1641
3.05(2)	2.997	2.526(3)	3.138(6)	2.763(3)	2.659(3)	0.13378	0.02303	30.5368	10.3373	9.2528	2.1572
4.06(1)	2.986	2.515(3)	3.107(5)	2.759(2)	2.637(2)	0.1473	0.02873	30.0968	10.2948	9.1841	2.1448
5.06(1)	2.979	2.509(3)	3.075(5)	2.757(2)	2.624(2)	0.14957	0.03444	29.7465	10.2395	9.1245	2.1467
6.10(2)	2.967	2.501(3)	3.040(5)	2.755(3)	2.611(3)	0.14816	0.04016	29.3609	10.1965	9.0845	2.1298
7.12(1)	2.960	2.496(3)	3.015(5)	2.746(3)	2.595(3)	0.14874	0.04355	28.9440	10.1552	9.0450	2.1290
8.13(1)	2.951	2.484(3)	3.002(5)	2.748(3)	2.580(3)	0.15892	0.05059	28.5718	10.0511	8.9787	2.1233
9.09(2)	2.944	2.479(3)	2.973(5)	2.741(2)	2.561(3)	0.16253	0.05574	28.1863	10.0236	8.9330	2.1171
10.06(2)	2.937	2.481(3)	2.943(5)	2.746(3)	2.554(3)	0.16169	0.06151	28.0518	9.9820	8.8936	2.1144
11.13(4)	2.928	2.458(3)	2.926(5)	2.738(3)	2.533(3)	0.15689	0.06897	27.3437	9.9615	8.8383	2.1030
12.20(5)	2.921	2.449(3)	2.901(5)	2.742(3)	2.515(3)	0.15774	0.07924	26.9568	9.9662	8.7889	2.1018
13.12(6)	2.915	2.441(3)	2.878(5)	2.740(3)	2.504(3)	0.16071	0.08361	26.6681	9.9353	8.7544	2.0995
14.06(5)	2.907	2.434(3)	2.864(5)	2.748(3)	2.496(3)	0.16365	0.08959	26.5247	9.8687	8.7430	2.0956
15.17(8)	2.900	2.431(3)	2.842(5)	2.747(3)	2.479(3)	0.15881	0.0985	26.1696	9.8470	8.6955	2.0920
16.07(9)	2.892	2.429(4)	2.817(6)	2.746(3)	2.465(3)	0.16213	0.10465	25.8551	9.8244	8.6671	2.0946
17.19(5)	2.884	2.416(3)	2.806(5)	2.754(3)	2.456(3)	0.16361	0.11172	25.6510	9.7649	8.6166	2.0875
17.94(3)	2.883	2.410(3)	2.790(5)	2.746(3)	2.446(3)	0.16337	0.11289	25.3744	9.7786	8.6052	2.0878
19.05(5)	2.872	2.408(3)	2.778(5)	2.749(3)	2.428(3)	0.16442	0.12336	25.0893	9.6541	8.5398	2.0798
19.9(1)	2.866	2.402(3)	2.741(5)	2.751(3)	2.413(3)	0.16164	0.13177	24.8286	9.6804	8.5187	2.0693
0.0001*	3.030	2.561(5)	3.245(8)	2.789(4)	2.712(4)	0.12565	0.00903	32.2089	10.5109	9.4280	2.1856

* after pressure release

differences in the compression of individual distances *X*-O4 and *X*-O1. Up to 20 GPa the *X*-O4 distance shortens by 1.2% in maruyamaite and by 2.5% in dravite. Even more subtle difference is observed for the *X*-O1 distance, which is also less compressible in maruyamaite (15%) as compared to dravite (16%). Interestingly, the *X*-O2 contact is considerably longer in maruyamaite than in dravite, but the slopes of *X*-O2 distance as a function of pressure are almost identical. As a result, at 20 GPa the difference in bulk compression of the *X* site in maruyamaite (22.8%) and dravite (23.4%) comprises only about half a percent. Note that the described minor distinctions become apparent at $P > 15$ GPa.

The B-O bonds are, along with the Si-O bonds, the most rigid, but their H*P* behaviour is not uniform in maruyamaite. The BO_3 group includes one B-O2 bond with the *Y* octahedron and two B-O8 bonds with *Z* octahedra (Fig. 1). Up to 9 GPa the B-O8 bond regularly shortens (Fig. 6), whereas the B-O2 bond does not change or even slightly increases; above 10 GPa both these bonds tend to diminish, but they become roughly equidistant only at 20 GPa. The same tendency is observed in dravite, but a detailed comparison is difficult here due to a large data spread (see Fig. 6).

To characterize the compression mechanism of tourmaline, several parameters describing the distortion of T_6O_{18} ring are used. The mentioned puckering of the T_6O_{18} ring (Fig. 1), measured by the distance between the O6 atom and threefold axis L_3 (Foit 1989), depends mainly on the contraction of the *Y* octahedra (O'Bannon et al. 2018). In our case the pressure dependence of the ring puckering (suppl. Fig. S3) is highly regular, in contrast to a minor deviation observed at about 10 GPa on the V/*P* curve of *Y* site (Fig. 4). Note a longer O6-L_3 distance in dravite (suppl. Fig. S3), implying a larger size of *Y* octahedron. This apparently agrees with the above mentioned different compressibility of the *Y* site in maruyamaite and dravite, reflecting different cation composition.

Two other parameters, the ditrigonality and crimping of T_6O_{18} ring, are shown to depend mainly on the *X* cation moving towards the ring (O'Bannon et al. 2018). Ditrigonality is defined as $\delta = (r_1 - r_s)/r_s$, where r_1 and r_s are the distances from O4 and O5, respectively, to the threefold axis (Barton 1969). Similarly to the ring puckering, the ditrigonality in maruyamaite increases regularly with pressure (suppl. Fig. S2), in accordance with regular change of the *X*-O distances (Fig. 5). Crimping, defined as $\Delta Z = [zO5-(zO4 + zO7)/2]*c$,

Table 3 The *R* 3 *m* unit cell parameters of maruyamaite as a function of pressure

P, GPa	*a*, Å	*c*, Å	V, Å^3
0.0001	15.941(3)	7.2269(14)	1590.43(50)
0.21(1)	15.920(3)	7.2046(14)	1581.4(5)
0.99(1)	15.905(3)	7.1825(14)	1573.5(5)
2.04(1)	15.882(3)	7.1515(14)	1562.2(5)
3.05(2)	15.853(3)	7.1157(14)	1548.8(5)
4.06(1)	15.817(3)	7.0817(14)	1534.3(5)
5.06(1)	15.797(3)	7.0550(14)	1524.7(5)
6.10(2)	15.764(3)	7.0218(14)	1511.2(5)
7.12(1)	15.748(3)	6.9993(14)	1503.3(5)
8.13(1)	15.717(3)	6.9703(14)	1491.2(5)
9.09(2)	15.689(3)	6.9458(14)	1480.5(5)
10.06(2)	15.670(3)	6.9248(14)	1472.6(5)
11.13(4)	15.636(3)	6.8962(14)	1460.2(5)
12.20(5)	15.617(3)	6.8731(14)	1451.6(5)
13.12(6)	15.599(3)	6.8532(14)	1444.2(5)
14.06(5)	15.581(3)	6.8331(14)	1436.6(5)
15.17(8)	15.558(3)	6.8158(14)	1428.7(5)
16.07(9)	15.544(3)	6.7977(14)	1422.4(5)
17.19(5)	15.516(3)	6.7748(14)	1412.5(5)
17.94(3)	15.507(3)	6.7649(14)	1408.7(5)
19.05(5)	15.468(3)	6.7385(14)	1396.2(5)
19.9(1)	15.448(3)	6.7208(14)	1389.0(5)
0.0001*	15.941(3)	7.2214(14)	1589.1(5)

* on pressure release

where z is the coordinate of O atoms and c is the length of the c-axis (Gorskaya et al. 1982), characterizes mutual rotation of the neighbor tetrahedra in the ring. The $\Delta Z/P$ curve has a pronounced bend at about 10 GPa (Fig. 7); above 10 GPa ΔZ remains roughly constant.

On the whole, within the range of 0–20 GPa the variations of the ring puckering, crimping and ditrigonality are very similar in maruyamaite and dravite, as it is seen from the data comparison in Figs. 7, S2 and S3. The same holds for the bulk compressibility of the *T* polyhedron, as well as for the majority of interatomic distances. The main difference is that the *Y* site is more rigid in maruyamaite; a minor but resolvable difference concerns a lesser compressibility of the *X* site (at $P > 15$ GPa) and a larger compressibility of the *Z* octahedron in maruyamaite.

Discussion

The obtained values of the bulk modulus of maruyamaite are the highest among those found for synthetic and natural alkali tourmalines (O'Bannon et al. 2018; Berryman et al. 2018),

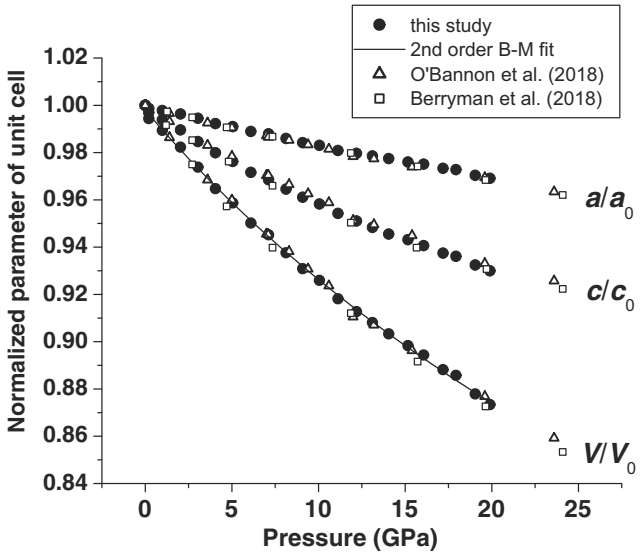

Fig. 3 Normalized axial and volume compression curves of maruyamaite in comparison with the data on dravite (O'Bannon et al. 2018) and cation-deficient synthetic K-dravite (the data points are compiled from Berryman et al. 2018). The line shows the 2nd order Burch-Murnaghan fit of the V/V_0 data points for maruyamaite

though the difference is quite minor. Since the Al content in synthetic K-dravite and in our sample is similar, the difference in the bulk modulus can be attributed to the presence of 40% of vacancies in the large *X* site of synthetic K-dravite. The compression anisotropy observed in maruyamaite agrees with the majority of the previous data on tourmaline compressibility and is very similar to that of dravite (O'Bannon et al. 2018) and synthetic K-dravite (Berryman et al. 2018). A minor

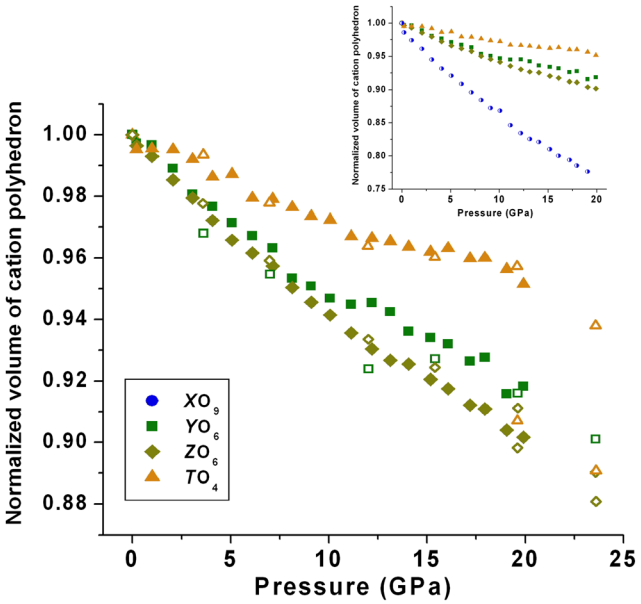

Fig. 4 The relative compressibilities of the main polyhedra in maruyamaite (solid symbols) and dravite (empty symbols, data compiled from O'Bannon et al. 2018) structure. The inset graph includes the compression curve for the largest *X* polyhedron

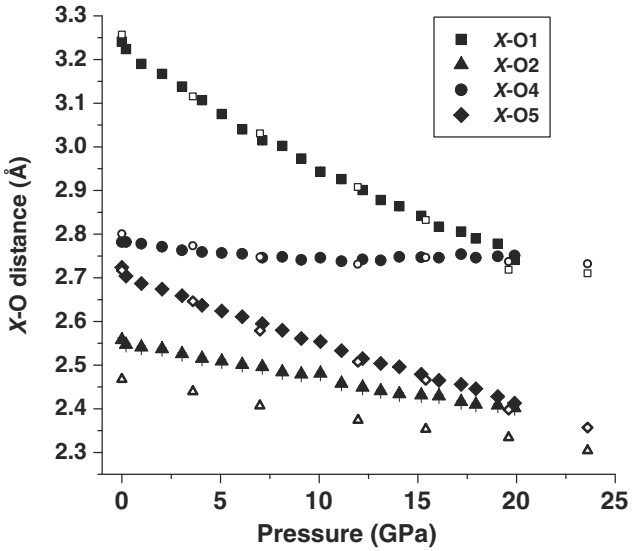

Fig. 5 Pressure dependences of the *X*-O distances in maruyamaite (solid symbols) and dravite (empty symbols, data compiled from O'Bannon et al. 2018) structure

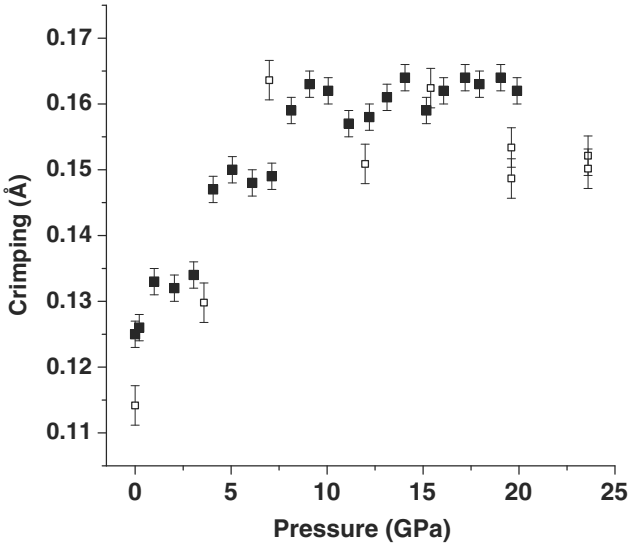

Fig. 7 Pressure dependence of the T_6O_{18} ring crimping in maruyamaite (solid symbols) and dravite (empty symbols, data compiled from O'Bannon et al. 2018) structure

increase of the c axial compressibility in both K-tourmalines, compared to dravite supports the mentioned correlation with the axial metric which can be seen from the comparative data on (Na,K)(Mg,Al) tourmalines (Berryman et al. 2018): the smaller the initial *c* parameter (more compressed structure), the lesser the compression.

Regarding the role of structural polyhedra in the reduction of bulk compressibility of maruyamaite compared to dravite, the inspection of Fig. 4 clearly demonstrates a dominant contribution of the *Y* octahedron. A higher rigidity of the Y site in maruyamaite is apparently due to the presence of significant amount of Al. The role of *X* site is negligible; for example, despite the *X*-O1 distance parallel to the c axis is less compressible in maruyamaite than in dravite (Fig. 5), it does not prevent a notably larger compressibility along this direction of maruyamaite.

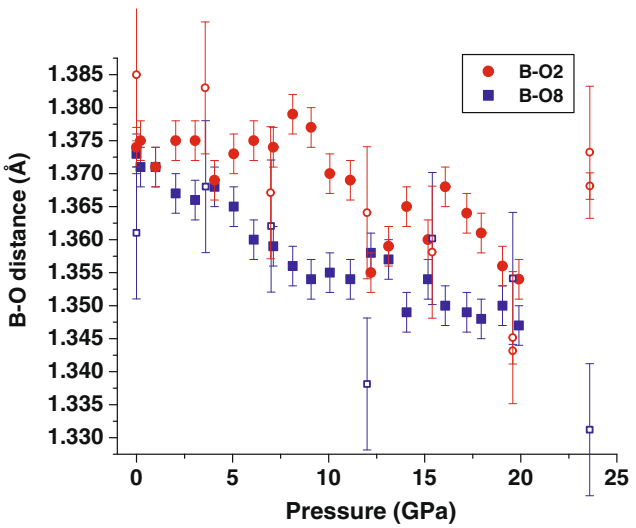

Fig. 6 Pressure dependences of the B-O distances in maruyamaite (solid symbols) and dravite (empty symbols, data compiled from O'Bannon et al. 2018) structure

An interesting point is a close similarity in the H*P* distortion of structure polyhedra, surrounding the *X* site, in maruyamaite and dravite. First of all this concerns the ditrigonality of T_6O_{18} ring. This parameter is known to strongly depend on the type of neighboring cation. For example, in the framework aluminosilicates with ANA type structure the 6-membered $(Si,Al)_6O_{18}$ rings, forming the channels along bodily diagonals of the cubic lattice, ditrigonalize under the influence of Na^+, but not K^+ (Seryotkin et al. 2005; Seryotkin and Bakakin 2008; Likhacheva et al. 2012). In maruyamaite the effect of large K cation onto ditrigonalization is apparently masked due to a mixed occupancy of the *X* site by Na and K, the cations with different bond valence requirements.

Nevertheless, since the displacement of the *X* cation to the T_6O_{18} ring is supposed to play role in the phase transition observed in dravite above 15.4 GPa (O'Bannon et al. 2018), we can infer a certain stabilizing influence of K onto the H*P* behaviour of maruyamaite. Despite the similarity in T_6O_{18} ring ditrigonality in both tourmalines at 20 GPa, the mean *X*-O distances, in particular the more rigid *X*-O4 contact with T_6O_{18} ring, remain slightly larger in maruyamaite, which apparently prevents the phase transition within 20 GPa. On the other hand, the existence of phase transition in maruyamaite at $P > 20$ GPa cannot be excluded, taking into account the mentioned similarities in overall structure evolution of the two minerals under pressure.

Regarding the role of cations occupying large voids in the structure of silicate minerals, it is worth to mention a well-known fact that in the framework silicates K and Na tend to have separate structural positions according to their different crystal chemical properties (Liebau 1985). Moreover, in some cases the charge balance and steric stabilization functions of K and Na can be distinguished. For example, in osumilite $(K,Na)(Mg,Fe)_2(Al,Fe)_3(Si,Al)_{12}O_{30}$ having a mixed framework, K is located near the 6-membered double ring and stabilizes the structure, whereas Na occupying a smaller void serves mainly for the charge balance (Seryotkin et al. 2008). In this respect the tourmaline structure presents quite a unique example of full mixing of cations with different properties in one (*X*) site. At that, large variation of the total occupancy of the *X* site in natural tourmalines (Hawthorne and Henry 1999) and steric stability of *X*-vacant varieties such as olenite (Berryman et al. 2018) suggests that the charge compensation predominates over stabilization function. Nevertheless, in alkali tourmaline we observe an "ordinary" stabilization effect produced by the replacement Na → K, though it is only minor. Note that, in agreement with the data of Berryman et al. (2018), the stabilization role of potassium in maruyamaite becomes apparent at high pressure, especially at $P > 15$ GPa. It is evinced in the absence of the H*P* phase transition within 15–20 GPa, probably due to the shift the transition onset to higher pressure.

A relatively high density of the presented structural data enables to reveal several additional features of polyhedra distortions, which demonstrate their complex interaction on compression. Non-uniform behaviour of the B-O bonds obviously reflects some difference in the compression of the neighbor *Y* and *Z* octahedra. The anomaly on the ring crimping curve observed at 10 GPa (Fig. 7) shows that this parameter depends not only on the *X* cation distance; the distortion of the neighbor octahedra can play a role here. Since the V/*P* curve for the *Y* octahedron (Fig. 4) also slightly deviates at about 10 GPa, we can infer that the mentioned anomalies of the B-O bonds and the ring crimping are influenced mainly by the *Y* site. We therefore observe some subtle change in the compression mechanism of tourmaline structure at 10 GPa within the present symmetry *R*3*m*. Most likely it is not a proper feature of maruyamaite behaviour, because similar *V*/P trend is observed for the *Y* site in dravite (O'Bannon et al. 2018). We can suppose that the observed change in the compression of the *Y* site has something in common with the luminescence anomaly reported by O'Bannon et al. (2018) within the nearest pressure range (at about 9 GPa).

Finally, we can briefly compare the H*P* behaviour of tourmaline and other 6-membered ring silicates, such as beryl $Be_3Al_2Si_6O_{18}$ and cordierite $(Mg,Fe)_2Al_4Si_5O_{18}$. A major similarity is the compression anisotropy: the orientation of rigid 6-membered rings makes the c-direction more compressible compared to the a-b plane in all three minerals. Interestingly, the presence of open channels in beryl and cordierite structure is apparently not critical for their overall rigidity, judging from relatively high bulk modulus of beryl (180.2 GPa, Prencipe et al. 2011) and cordierite (131 GPa, Miletich et al. 2014a) compared to tourmaline. On the other hand, the open channel topology provides more possibility for the distortion of 6-membered rings, which is manifested by drastic framework deformations upon the phase transitions in cordierite at about 7 and 15 GPa (Miletich et al. 2014a,b; Finkelstein et al. 2015). The absence of extensive deformations in beryl (Prencipe et al. 2011; O'Bannon and Williams 2016) clearly shows their strong dependence on the cation composition of tetrahedral and octahedral sites.

In tourmaline the tetrahedral units make a lesser part of the framework compared to beryl and cordierite, and the compression mechanism is mainly governed by the octahedral sites, which are softer than tetrahedra and thereby provide a larger compressibility for tourmaline. But, due to a different topology of tourmaline structure, the relative distortions of the framework units are smaller compared to the channel silicates beryl and cordierite.

Conclusions

A single crystal diffraction study of maruyamaite reveals no sharp distinction with the structural behaviour of dravite regarding the compression anisotropy and the evolution of the main structure parameters. A slightly higher bulk modulus of maruyamaite is mainly caused by the presence of Al in octahedral site *Y*. However, a minor change in the rigidity of local contacts of the *X* site with T_6O_{18} ring, due to the presence of K, is apparently critical for stabilization of maruyamaite structure. This is evinced by the absence of the phase transition in maruyamaite within 15–20 GPa, in contrast to dravite. The stabilizing function of K becomes apparent at $P > 15$ GPa, in accordance with the recent findings of Berryman et al. (2018).

A mixed occupation of the large *X* site by such different cations as Na and K apparently restricts specific distortions in tourmaline structure, which could fulfill the bond valence requirements of an individual cation. This seems to be the reason for the "invariance" of the pressure-induced changes in the structure polyhedra, surrounding the *X* site, in maruyamaite and dravite.

Acknowledgements The authors are grateful to J. Cempírek and an anonymous reviewer for their helpful remarks, as well as to Yu.V. Seryotkin for valuable discussion of the results. This study is supported by the Russian Scientific Foundation (project 18-17-00186). Diffraction experiments were carried at the European Synchrotron Radiation Facility and supported by approval of ESRF Proposal ES-810.

References

Agilent (2012) CrysAlis PRO. Agilent Technologies, Yarnton

Angel RJ, Gonzalez-Platas J, Alvaro M (2014) EosFit-7c and a Fortran module (library) for equation of state calculations. Z Kristallogr 229: 405–419

Barton R (1969) Refinement of the crystal structure of buergerite and the absolute orientation of tourmalines. Acta Cryst B25:1524–1533

Berryman EJ, Wunder B, Rhede D (2014) Synthesis of K-dominant tourmaline. Am Mineral 99:539–542

Berryman EJ, Wunder B, Wirth R, Rhede D, Schettler G, Franz G, Heinrich W (2015) An experimental study on K and Na incorporation in dravitic tourmaline and insight into the formation environment of diamoniferous tourmaline from the Kokchetav, Massif, Kazakhstan. Contrib Mineral Petrol 169:28

Berryman EJ, Wunder B, Ertl A, Koch-Müller M, Rhede D, Scheidl K, Giester G, Heinrich W (2016) Influence of the X-site composition on tourmaline's crystal structure: investigation of synthetic K-dravite, dravite, oxy-uvite, and magnesio-foitite using SREF and Raman spectroscopy. Phys Chem Miner 43:83–102

Berryman EJ, Zhang D, Wunder B, Duffy TS (2018) High-pressure compressibility of synthetic tourmaline of near end-member compositions. AGU 2018 Abstracts

Bloodaxe ES, Hughes JM, Dyar MD, Grew ES, Guidotti CV (1999) Linking structure and chemistry in the Schorl-Dravite series. Am Mineral 84:922–928

Capillas C, Tasci ES, de la Flor G, Orobengoa D, Perez-Mato JM, Aroyo MI (2011) A new computer tool at the Bilbao Crystallographic Server to detect and characterize pseudosymmetry. Z Kristallogr 226:186–196

Dietrich RV (1985) The tourmaline group. Van Nostrand Reinhold Company Inc., New York

Dutrow BL, Henry DJ (2011) Tourmaline: A geologic DVD. Elements 7: 301–306

Finkelstein GJ, Dera PK, Duffy TS (2015) High-pressure phases of cordierite from single-crystal X-ray diffraction to 15 GPa. Am Mineral 100:1821–1833

Foit FF (1989) Crystal chemistry of alkali-deficient schorl and tourmaline structural relationships. Am Mineral 74:422–431

Gorskaya MG, Frank-Kamenetskaya OV, Rozhdestvenskaya IV, Frank-Kamenetskii VA (1982) Refinement of the crystal structure of Al-rich elbaite, and some aspects of the crystal chemistry of tourmalines. Soviet Physics Crystallogr 27:6

Hawthorne FC (2002) Bond-valence constraints on the chemical composition of tourmaline. Can Mineral 40:789–797

Hawthorne FC, Dirlam DM (2011) Tourmaline, the indicator mineral: From atomic arrangement to Viking navigation. Elements 7:307–312

Hawthorne FC, Henry DJ (1999) Classification of the minerals of the tourmaline group. Eur J Mineral 11:201–215

Hawthorne FC, MacDonald DJ, Burns PC (1993) Reassignment of cation site-occupancies in tourmaline: Al/Mg disorder in the crystal structure of dravite. Am Mineral 78:265–270

Henry DJ, Dutrow BL (1996) Metamorphic tourmaline and its petrologic applications. Rev Mineral 33:503–557

Henry DJ, Novák M, Hawthorne FC, Ertl A, Dutrow BL, Uher P, Pezzotta F (2011) Nomenclature of the tourmaline super-group minerals. Am Mineral 96:895–913

Hezel DC, Kalt A, Marschall HR, Ludwig T, Meyer H-P (2011) Major-element and Li, Be compositional evolution of tourmaline in an Stype granite–pegmatite system and its country rocks: an example from Ikaria, Aegean Sea, Greece. Can Mineral 49:321–340

Hwang SL, Shen P, Chu HT, Yui TF, Liou JG, Sobolev NV, Shatsky VS (2005) Crust-derived potassic fluid in metamorphic microdiamond. Earth Planet Sci Lett 231:295–306

Li H, Qin S, Zhu X, Liu J, Li X, Wu X, Wu Z (2004) In situ high-pressure X-ray diffraction of natural tourmaline. Nuclear techniques 27:919–922

Liebau F (1985) Structural Chemistry of the Silicates. Structure, Bonding, and Classification. Springer-Verlag, Berlin

Likhacheva AY, Rashchenko SV, Seryotkin YV (2012) The deformation mechanism of pressure-induced phase transition in dehydrated analcime. Mineral Mag 76:129–142

Ludwig T, Marschall HR, Pogge von Strandmann PAE, Shabaga BM, Fayek M, Hawthorne FC (2011) A secondary ion mass spectrometry (SIMS) re-evaluation of B and Li isotopic compositions of Cu-bearing elbaite from three global localities. Mineral Mag 75:2485–2494

Lussier AJ, Aguiar PM, Michaelis VK, Kroeker S, Herwig S, Abdu Y, Hawthorne FC (2008) Mushroom elbaite from the Kat Chay mine, Momeik, near Mogok, Myanmar: I. Crystal chemistry by SREF, EMPA, MAS NMR and Mössbauer spectroscopy. Mineral Mag 72:747–761

Lussier AJ, Abdu Y, Hawthorne FC, Michaelis VK, Aguiar PM, Kroeker S (2011) Oscillatory zoned liddicoatite from Anjanabonoina, central Madagascar. I. Crystal chemistry and structure by SREF and 11B and 27Al MAS NMR spectroscopy. Can Mineral 49:63–88

Lussier AJ, Hawthorne FC (2011) Oscillatory zoned liddicoatite from central Madagascar. II. Compositional variations and substitution mechanisms. Can Mineral 49:89–104

Lussier AJ, Ball NA, Hawthorne FC, Henry DJ, Shimizu R, Ogasawara Y, Ota T (2016) Maruyamaite, K(MgAl2)(Al5Mg)Si6O18(BO3)3(OH)3O, a potassium-dominant tourmaline from the ultrahigh-pressure Kokchetav massif, northern Kazakhstan: Description and crystal structure. Am Mineral 101:355–361

MacDonald DJ, Hawthorne FC (1995) The crystal chemistry of Si <–-> Al substitution in tourmaline. Can Mineral 33:849–858

Mao HK, Xu J, Bell PM (1986) Calibration of the ruby pressure gauge to 800 kbar under quasi-hydrostatic conditions. J Geophys Res 91: 4673–4676

Marschall HR, Ludwig T, Altherr R, Kalt A, Tonarini S (2006) Syros metasomatic tourmaline: Evidence for very high-d11B fluids in subduction zones. J Petrol 47:1915–1942

Marschall HR, Jiang S-Y (2011) Tourmaline Isotopes: No element left behind. Elements 7:313–319

Martin RF (2011) Can Mineral 49, pp 1–405

Merlini M, Hafland M (2013) Single-crystal diffraction at megabar conditions by synchrotron radiation. High Pressure Res 33:511–522

Meyer C, Wunder B, Meixner A, Romer RL, Heinrich W (2008) Boron isotope fractionation between tourmaline and fluid: an experimental re-investigation. Contrib Mineral Petrol 156:259–267

Miletich R, Gatta GD, Willi T, Mirwald PW, Lotti P, Merlini M (2014a) Cordierite under hydrostatic compression: anomalous elastic behavior as a precursor for a pressure-induced phase transition. Am Mineral 99:479–493

Miletich R, Scheidl KS, Schmitt M, Moissl AP, Pippinger T, Gatta GD, Schuster B, Trautmann C (2014b) Static elasticity of cordierite I: effect of heavy ion irradiation on the compressibility of hydrous cordierite. Phys Chem Miner 41:579–591

Novák M, Škoda P, Filip J, Macek I, Vaculovič T (2011) Compositional trends in tourmaline from intragranitic NYF pegmatites of the Třebíč Pluton, Czech Republic; electron microprobe, Mössbauer and LA-ICP-MS study. Can Mineral 49:359–380

O'Bannon E, Beavers CM, Kunz M, Williams Q (2018) High-pressure study of dravite tourmaline: Insights into the accommodating nature of the tourmaline structure. Am Mineral 101:1622–1633

O'Bannon E, Williams Q (2016) Beryl-II, a high-pressure phase of beryl: Raman and luminescence spectroscopy to 16.4 GPa. Phys Chem Miner 43:671–687

Ota T, Kobayashi K, Kunihiro T, Nakamura E (2008a) Boron cycling by subducted lithosphere; insights from diamondiferous tourmaline

from the Kokchetav ultrahigh-pressure metamorphic belt. Geochim Cosmochim Acta 72:3531–3541

Ota T, Kobayashi K, Katsura T, Nakamura E (2008b) Tourmaline breakdown in a pelitic system: implications for boron cycling through subduction zones. Contrib Mineral Petrol 155:19–32

Pertlik F, Ertl A, Körner W, Brandstätter F, Schuster R (2003) Na-rich dravite in the marbles from Friesach. Chemistry and crystal structure. Neues Jahrbuch für Mineralogie Monatshefte, Carinthia, pp 277–288

Petříček V, Dušek M, Palatinus L (2014) Crystallographic Computing System JANA2006: General features. Zeitschrift für Kristallographie - Crystalline Materials 229:345–352

Prencipe M, Scanavino I, Nestola F, Merlini M, Civalleri B, Bruno M, Dovesi R (2011) High-pressure thermo-elastic properties of beryl (Al4Be6Si12O36) from ab initio calculations, and observations about the source of thermal expansion. Phys Chem Miner 38:223–239

Rothkirch A, Gatta GD, Meyer M, Merkel S, Merlini M, Liermann H-P (2013) Single-crystal diffraction at the Extreme Conditions beamline P02.2: procedure for collecting and analyzing high-pressure single-crystal data. J Synchrotron Radiat 20:711–720

Seryotkin YV, Bakakin VV, Bazhan IS (2005) The structure of dehydrated (Li0.7Na0.3)-analcime: a trigonal deformation of the framework and new low-coordinated non-framework positions. J Struct Chem 46:681–693

Seryotkin YV, Bakakin VV (2008) The thermal behavior of secondary analcime and leucite derivate and its structural interpretation. Russ Geol Geophys 49:207–213

Seryotkin YV, Sokol EV, Bakakin VV, Likhacheva AY (2008) Pyrometamorphic osumilite: occurrence, paragenesis, and crystal structure as compared to cordierite. Eur J Mineral 20:191–198

Shannon RD (1976) Revised effective ionic radii and systematic studies of interatomic distances in halides and chalcogenides. Acta Crystallogr A 32:751–776

Sheldrick GM (2008) A short history of SHELX. Acta Crystallogr A64: 112–122

Schertl H-P, Sobolev NV (2013) The Kokchetav Massif, Kazakhstan: "Type locality" of diamond bearing UHP metamorphic rocks. J Asian Earth Sci 63:5–38

Shimizu R, Ogasawara Y (2005) Discovery of K-tourmaline in diamond-bearing quartz-rich rock from the Kokchetav Massif, Kazakhstan. Mitteilungen der Österreichischen Mineralogischen Gesellschaft 150:141

Shimizu R, Ogasawara Y (2013) Diversity of potassium-bearing tourmalines in diamondiferous Kokchetav UHP metamorphic rocks: a geochemical recorder from peak to retrograde metamorphic stages. J Asian Earth Sci 63:39–55

van Hinsberg V, Henry DJ, Marschall HR (2011) Tourmaline: an ideal indicator of its host environment. Can Mineral 49:1–16

van Hinsberg VJ, Schumacher JC (2007) Using estimated thermodynamic properties to model accessory phases: the case of tourmaline. J Metamorph Geol 25:769–779

Xu J, Kuang Y, Zhang B, Liu Y, Fan D, Li X, Xie H (2016) Thermal equation of state of natural tourmaline at high pressure and temperature. Phys Chem Miner 43:315–326